Investigations of Large-Scale Voltage-Dependent Loads for Damping Inter-Area Oscillations: Mechanism and Robust Decentralized Control

Chen Zhang, *Student Member, IEEE*, Deping Ke, Yuanzhang Sun, *Senior Member, IEEE*, C. Y. Chung, *Fellow, IEEE*, Jian Xu, *Member, IEEE*

***Abstract*—To uncover the mechanism by which voltage-dependent loads (VDLs) influence electromechanical dynamics, this paper mathematically deduces the damping torque induced by VDLs based on a single machine infinite bus system. Moreover, by continuously regulating the terminal voltage of a typical large-scale VDL, i.e., the aluminum electrolysis load, this paper proposes a novel load damping control architecture to dynamically modulate the power consumption of controlled loads so as to eliminate inter-area oscillations in power systems. Specifically, the decentralized load damping controllers (LDCs) used in this architecture are designed by a proposed multi-stage mixed H_2/H_∞ control approach to guarantee robustness against uncertainties (e.g., tie-line outages, wind generation fluctuations) as well as to ensure reasonable control efforts of controlled VDLs. Simulation results on the modified New England and New York interconnected system validate the method for analysis of VDLs' effects on inter-area oscillations and show the proposed load damping control strategy can satisfactorily damp inter-area oscillations over multiple operating points.**

***Index Terms*—Large-scale voltage-dependent load, inter-area oscillations, load damping control, robust decentralized control.**

I. Introduction

INTER-AREA oscillations are longstanding and challenging security issues in power systems due to their association with groups of components that are usually distributed and up to hundreds of miles away. The voltage-dependent load (VDL) significantly influences inter-area oscillations. Based on the modal analysis and nonlinear time-domain simulations, [1] and [2] explored the influence of VDLs on electromechanical oscillations and observed they are highly related to the loaded conditions of the system and the types of excitation systems employed.

A. Load Control for Damping

Although VDLs have been widely studied for primary frequency control and voltage stability [3]-[6], their architecture and techniques concerning their control to alleviate inter-area oscillations are rarely reported. Reference [7] gave the earliest outline of the general framework to improve angle stability by modulating the power of some conceptually controllable loads. Furthermore, Kamwa *et al.* [8], [9] used multi-band stabilizers to conduct constructive and inspiring work on shedding the active power of loads to enhance stability of the frequency and electromechanical oscillations. Besides, an anticipated control strategy was proposed in [10] to dispatch the steady-state power consumption of loads, rather than dynamically modulate the loads' power, so that the operating point is regulated to damp inter-area oscillations. However, these studies utilize loads without considering the necessary models and constraints thereof, possibly leading to undesirable control effects in practical applications. For example, [9] pointed out that certain loads might be ineffectively modulated in the most unstable cases due to strong oscillations of the bus voltage.

The authors' team has concentrated for many years on academic studies and industrial applications of direct load control techniques, specifically those based on aluminum electrolysis loads (AELs) that are quite sensitive to voltage [4], [5], [11]. The industrial AEL, as a typical representative of large-scale controllable VDLs in power systems, has two major merits that benefit power system dynamics: 1) the power consumption of the AEL can be rapidly and smoothly modulated by regulating its terminal voltage when series magnetically controlled reactors (MCRs) are installed; 2) the normal AEL operates with a fairly large and steady daily power consumption (usually up to hundreds of MWs) but it can endure terminal voltage deviations of ±10% for hours, which means it can offer considerable modulable active power to engage in dynamics control. Therefore, it is readily inferred that the control bandwidth based on the AEL can not only cover the widely studied primary frequency control issues [5], [11] but also the control problems associated with faster system dynamics, i.e., inter-area power oscillations in this paper.

B. Contributions

Besides the inadequate investigation on characteristics and models of the controlled loads, previous studies (e.g. [7]-[9]) of relevance also have little consideration towards the damping controllers' robustness in nowadays power systems. For example, the influences of operating point drifts (e.g. caused by wind power generation) on the damping control design have been addressed in [12]-[14]. In addition, those studies have not provided effective approach to constrain the damping controllers' control efforts although it is well known that excessive control efforts may remarkably deteriorate the dynamics of controlled VDLs.

By using the AEL as a specific example, this paper proposes to supplementarily control the large-scale VDL to suppress

This work was supported by the National Natural Science Foundation of China under Grant 51777143.

C. Zhang, D. Ke (corresponding author), Y. Sun, and J. Xu are with the School of Electrical Engineering, Wuhan University, Wuhan 430072, China (e-mail: eezhangchen@whu.edu.cn; kedeping@whu.edu.cn).

C. Y. Chung is with the Department of Electrical and Computer Engineering, University of Saskatchewan, Saskatoon, SK S7N 5A9, Canada (e-mail: c.y.chung@usask.ca).

inter-area oscillations in power systems. Similar to other damping control implemented based on, e.g., HVDC [15], FACTS devices [16], and energy storage systems (ESSs) [17], supplementary load damping controllers (LDCs) using wide-area feedback signals as the inputs are installed in the VDLs (AELs). Furthermore, compared to the above-mentioned studies associated with load control, this paper is the first to systematically address the use of large-scale VDLs to suppress inter-area oscillations in detail with respect to aspects of the mechanism and damping control system. The main three contributions of this paper are summarized as follows:

1) Based on the classical single machine infinite bus (SMIB) system, the transfer function between the damping torque and the VDL is first deduced so as to mathematically explain the phenomenon that the loaded condition of the power system and the types of excitation systems employed can differentially affect the influence of the VDL on the electromechanical oscillation, as observed in [1] and [2].

2) A novel wide-area load damping control architecture is proposed. By establishing the concrete model of AELs, its terminal voltage can be regulated by the series MCR. Thus, by virtue of wide-area measurement systems (WAMS), the proposed LDCs can synthesize the wide-area closed-loop control system and continuously modulate the power consumption of the AELs to suppress inter-area oscillations.

3) Because the AELs are generally distributed in distant areas, this paper proposes a multi-stage mixed H_2/H_∞ robust control approach to design the LDCs with a decentralized architecture. The coordinated LDCs can effectively and robustly suppress inter-area oscillations against uncertainties in practical power systems (e.g., tie-line outages, wind generation fluctuations).

The remainder of this paper is organized as follows. Detailed analysis and discussion of the effects of VDLs are illustrated in Section II. Sections III and IV respectively introduce the wide-area load damping control strategy and the robust LDC design procedure. Simulations of the modified New England and New York interconnected system are conducted in Section V. Finally, Section VI concludes the paper.

II. Effects of the VDL Characteristics

A. Modified SMIB System

To explore the general mechanism of the influence of VDLs on electromechanical oscillations, the SMIB system is employed as shown in Fig. 1. A third-order synchronous generator and a high gain static exciter (AVR) are adopted in this system. The local load VL at the terminal bus is voltage dependent. In addition, the power output of the generator P_G is divided into two parts: P_L consumed by the local load VL and P_T transmitted to the infinite bus through a tie-line.

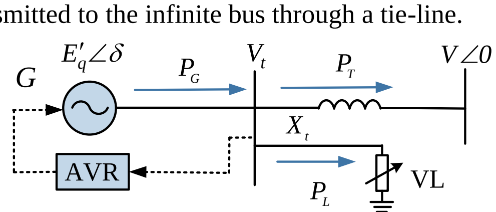

Fig. 1. The SMIB integrated with a voltage-dependent load.

To simplify the analysis, it is assumed that the load VL only consumes active power and its voltage-dependent characteristic can be represented by a general exponential form [18]:

$$P_L(V_t) = P_0\left(\frac{V_t}{V_0}\right)^{\alpha} \tag{1}$$

where P_0 and V_0 denote the nominal values of the load's active power and terminal voltage, respectively; V_t is the actual terminal voltage; and α is the exponent. This mathematical model can be employed to depict constant power (CP), constant current (CC), and constant impedance (CI) load types by setting α to be 0, 1, and 2, respectively.

The nonlinear dynamic model of the SMIB system is linearized around the nominal operating point, and the deviations of the electromagnetic torque ΔM_e, the transient voltage $\Delta E'_q$, the terminal voltage ΔV_t, and the load power ΔP_L can be computed as follows:

$$\begin{cases} \Delta M_e = K_1\Delta\delta + K_2\Delta E'_q \\ \Delta E'_q = G_3\left(\Delta E_{fd} - K_4\Delta\delta\right) \\ \Delta V_t = K_5\Delta\delta + K_6\Delta E'_q \\ \Delta P_L = K_L\Delta V_t \end{cases} \tag{2a}$$

$$G_3 = \frac{K_3}{1+K_3T'_{d0}s},\ \ \Delta E_{fd} = -G_e\Delta V_t = -\frac{K_A}{1+T_e s}\Delta V_t,\ \ K_L = \alpha\frac{P_0}{V_0} \tag{2b}$$

where K_1~K_6 are the commonly used coefficients in the small-signal stability analysis, and their detailed calculations are presented in Appendix A [18]-[20]; ΔE_{fd} is the deviation of the exciter's output voltage; T'_{d0} is the d-axis open-circuit transient time constant; K_A and T_e are the gain and time constant of the exciter, respectively; and K_L represents the sensitivity of the load power with respect to the terminal voltage.

Substituting (2b) into (2a) yields the open-loop transfer function from the deviation of the power angle $\Delta\delta$ to ΔV_t:

$$G_V(s) = \frac{\Delta V_t}{\Delta\delta} = \frac{K_5 - K_4K_6G_3}{1+K_6G_eG_3} \tag{3}$$

Generally, the gain K_A of an exciter in modern power systems is fairly large and its time constant T_e is very small. Thus, the transfer function (3) can be further simplified:

$$G_V(s) \approx K_5 - \frac{K_6(K_4+K_5K_A)}{K_6K_A + T'_{d0}s} \tag{4}$$

Similarly, based on (2), the open-loop transfer function $\Delta\delta\to\Delta P_L$ can be deduced:

$$G_L(s) = \frac{\Delta P_L}{\Delta\delta} = K_L\left(K_5 - \frac{K_6(K_4+K_5K_A)}{K_6K_A + T'_{d0}s}\right) \tag{5}$$

Using the complex torque method, [18] investigated the mechanism of the excitation system in detail. This paper depends on its work and additionally introduces a feedback loop ($\Delta\delta\to\Delta M_L$) to investigate the electromagnetic torque ΔM_L induced by the voltage-dependent load VL, as shown in Fig. 2. Routinely, ΔM_L is orthogonally decomposed into the synchronizing torque ΔM_{LS} and the damping torque ΔM_{LD} in the complex plane, as follows:

$$\Delta M_L = \Delta P_L = \Delta M_{LS}\Delta\delta + \Delta M_{LD}\Delta\omega \tag{6a}$$

$$\begin{cases} \Delta M_{LS} = \dfrac{K_L\left(K_5 T_{d0}'^2 \omega^2 \text{-} K_4 K_6^2 K_A\right)}{K_6^2 K_A^2 + T_{d0}'^2 \omega^2} \\ \Delta M_{LD} = \dfrac{K_L K_6 T_{d0}' (K_4 + K_5 K_A)}{K_6^2 K_A^2 + T_{d0}'^2 \omega^2} \end{cases} \tag{6b}$$

Therefore, the phase shift from $\Delta\delta$ to ΔM_L (caused by $G_V(s)$) is critical for the load to produce damping torque. According to (5) and (6), the system component parameters and the operating point primarily determine the phase shift and thus the load's damping effect, which will be discussed in detail in the following.

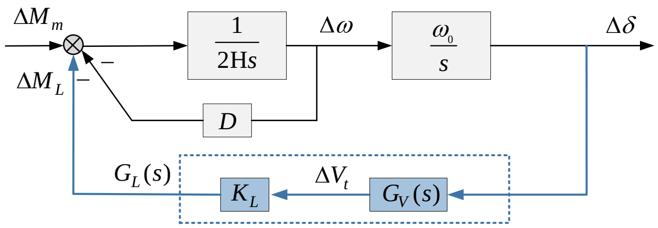

Fig. 2. Electromagnetic torque induced by the VDL.

B. Discussion

Generally, the synchronizing torque impacting the transient stability is adequate in modern power systems due to the high gain and sensitive AVR [18], and is not of special concern in this paper. However, the situation becomes complicated for the damping torque and requires detailed investigations.

It is found from (6) that the sign of ΔM_{LD} is mainly decided by the parameter K_5 because the other parameters are always positive [18]. Appendix A shows that K_5 can be a positive or negative number, and its sign depends on the operating point and the system's structure and parameters. ΔM_{LD} will be positive with a positive K_5, indicating that the load induces a positive damping torque and is beneficial to the electromechanical oscillation dynamics (Fig. 3). In contrast, if K_5 is negative and $K_4+K_5K_A<0$, the load will have adverse effects on damping power oscillations compared to the previous case. Moreover, the adverse effects will be seriously amplified by K_A and K_L in (6). As mentioned in [18] and [20], negative K_5 easily emerges in stressed operating conditions such as transmitting heavy power over long-distance tie-lines. Under such stressed conditions, the VDL would therefore deteriorate damping ratios of the oscillation modes and lead to insufficient damping performance in power systems.

Although the stressed operating conditions will force the VDL to be adverse to small-signal stability, it is inferred that the phase of the torque induced by the VDL can be rotated by reasonably regulating its terminal voltage so that positive damping effects are produced. Specifically, this auxiliary terminal voltage control for VDLs can induce a supplementary positive damping torque ΔM_{SD} (green arrow in Fig. 3) and thus be beneficial for suppressing electromechanical oscillations in power systems. The detailed control architecture is introduced in the following section.

In particular, the main purpose of utilizing SMIB system is to clearly illustrate the way on which VDLs impact the electromechanical oscillations' damping. Indeed, there will be no theoretical difficulty to perform the induced damping torque analysis in a multi-machine system. For example, [21] deduces the damping torque which are induced by FACTS devices in a multi-machine system. The investigation results based on the SMIB system or multi-machines will make no essential difference. Thus, this paper will subsequently employ a multi-machine system to further confirm the correctness of the above investigation.

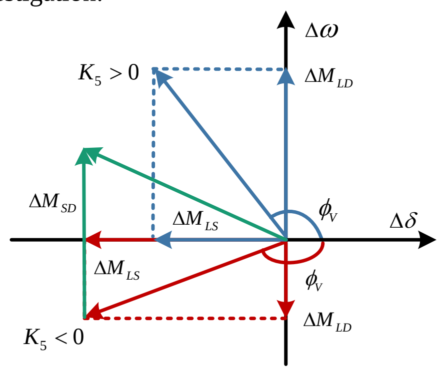

Fig. 3. A phasor diagram of torque ΔM_L with positive and negative K_5.

III. Proposed VDL-Based Load Damping Control Framework

Compared to previous works [7]-[10], this paper is the first to propose in detail a novel load damping control architecture for the VDL and specifically assess the damping capabilities of controlled VDLs. The strategy can not only mitigate the adverse effects from the VDL but also effectively suppress inter-area oscillations in power systems.

A. Basic Principle and Architecture

In modern power systems, many types of VDLs can commonly tolerate wide and frequent variations of supplied voltage [3]. In this paper, a typical example of such a large-scale VDL, the AEL (powered by DC voltage) [4], is specifically studied. Furthermore, industrial AELs in China have been gradually subjected to technical improvements to equip the MCRs, which are in series with the AELs, to regulate their terminal voltage. Specifically, MCRs have the advantages of good reliability, large capacity, and high voltage [22], [23]. Moreover, an AEL's terminal voltage can be smoothly and quickly adjusted by the MCR. In this paper, the series MCRs provide a convenient way to engage AELs in dynamics control because they can also rapidly respond to supplementary damping control signals.

Based on the feasibility of implementing supplementary control of the AELs accompanied by MCRs, this paper further proposes to reshape the natural damping characteristics of the AEL for suppressing inter-area oscillations of power systems. Fig. 4 shows the proposed wide-area damping control architecture based on the AELs. Briefly, the LDCs receive remote feedback signals from the WAMS center and generate auxiliary input signals to control the rectifier of the MCRs.

Moreover, Fig. 5 depicts the detailed series framework and control blocks of controlled AELs. When inter-area oscillations occur in power systems, wide-area input signals will be delivered to LDCs and then damping output signals Δu are added to a series thyristor-controlled rectifier for MCRs to change the series impedance ΔX between a public bus PB and a load terminal bus TB (the transfer function $G_M(s)$ for the MCRs is seen in [22]). Thus, the terminal voltage V_A will be regulated by ΔV_D and, consequently, the controlled AEL is continuously modulated to provide damping efforts to inter-area oscillations. After inter-area oscillations subside, LDCs will not be active and controlled AELs would return to the original steady state.

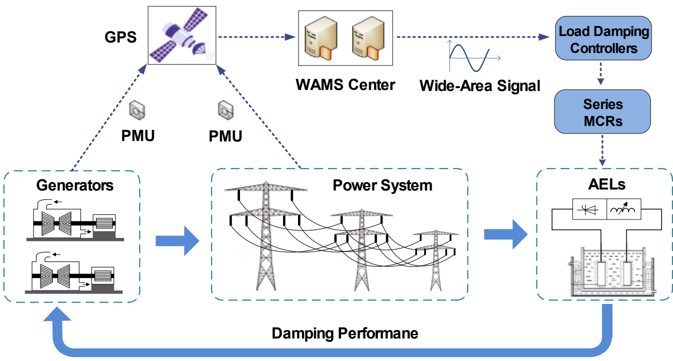

Fig. 4. The proposed wide-area closed-loop control structure.

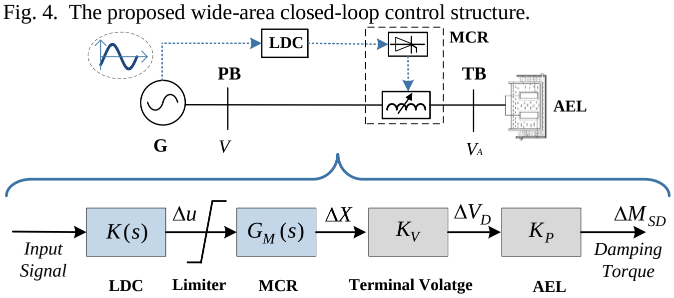

Fig. 5. The basic framework of proposed control.

B. Available Active Power Capacity of the AEL for Damping Control

For practical considerations, the LDC output magnitude should be limited to prevent excessively exerting the AEL and ensure the quality production of aluminum. With this limitation (shown in Fig. 5), it is therefore necessary to assess the available active power capacity provided by AELs for damping control. Generally, the active power P_A consumed by the AEL can be calculated as follows:

$$P_A = aV_A^2 + bV_A \tag{7}$$

where a and b are coefficients depending on the resistance and electromotive force of the AEL model, and V_A is the terminal voltage of the AEL. For example, [11] uses actual measurements to identify values of a and b of 4.96 and −1.66, respectively. Moreover, the nominal power of the AEL is 330 MW at V_A=1.0 p.u. Thus, as V_A is permitted to vary between 0.9 and 1.1 p.u., the power consumption of the AEL has a minimum of 252 MW and maximum of 417 MW; this indicates that up to ±20% of the AEL's active power capacity is available for power modulation to serve in the damping control. Hence, considering that the nominal capacities of AELs are usually quite large, they can definitely spare adequate dynamically controllable capacity to improve power system stability. In other words, similar to the characteristic of energy storage systems, the controlled AELs also have the potential to offer active power modulation to eliminate inter-area oscillations. Furthermore, the location of an AEL (or other types of VDLs) is another important factor to influence its capability for controlling electromechanical dynamics. In fact, where the industrial VDLs with large capacities are placed primarily depends on the practical needs and requirements. For example, AELs are generally sited close to aluminum mines. For simplicity, this paper however concentrates on the design of LDCs which modulate the power of VDLs, and it is assumed that the studied VDLs have the locations which will not affect their capabilities in controlling the electromechanical oscillations.

It should be noted that this paper mainly aims to investigate the mechanism by which VDLs influence electromechanical dynamics and further to propose a novel load damping control strategy to dynamically modulate the power consumptions of controlled VDLs so as to suppress inter-area oscillations in power systems. Specifically, both the mechanism investigation and subsequent robust damping control design are presented based on general VDL models which can be flexibly specialized to a variety of VDLs in practice, such as electrolysis loads [4], LED lighting [6], and electric water heating [24]. Namely, the proposed control strategy can be compatibly applied to these VDLs if providing detailed load models. Therefore, the AEL which is a specific yet typical VDL is employed in this paper to complete the exemplary demonstration of the proposed investigation and control design method.

IV. Multi-Stage Robust Design Strategy for Decentralized LDCs

A. Multi-Stage Robust Design Strategy

A robust design strategy mainly aims to enhance the robustness of LDCs against external disturbances and model uncertainties, such as tie-line outages and wind generation fluctuations. In this paper, a mixed H_2/H_∞ output-feedback control approach is used to achieve the multi-objective robust control purpose [25]. Moreover, H_∞ control can guarantee stability of a closed-loop system against uncertainties while H_2 control can optimize transient responses of the system, e.g., the control efforts of controllers [26]. Meanwhile, the required damping effects are fulfilled by implementing constraints on the placement of closed-loop poles in the control design. In addition, linear matrix inequality (LMI) optimization is a powerful and mature tool currently used to solve linear control problems.

The detailed configuration of the proposed design control strategy is depicted in Fig. 6. $G(s)$ is the transfer function of the open-loop power system and $K(s)$ represents the transfer function of the LDCs to be designed. Due to the utilization of wide-area feedback signals, the transmission time delay (τ) should be taken into account during the control design; thus, it is approximated in this paper by the second-order Pade formula ($D(s)$) which is simple yet more accurate than the first-order Pade formula for approximating time delays associated with the wide-area damping control, as follow:

$$e^{-\tau s} \approx \frac{\tau^2 s^2 - 6\tau s + 12}{\tau^2 s^2 + 6\tau s + 12} \tag{8}$$

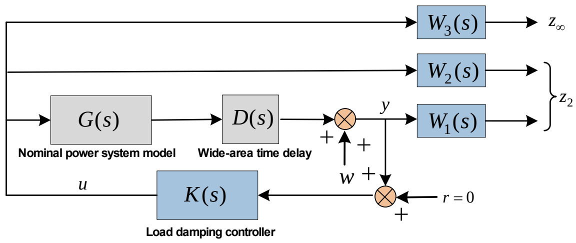

Fig. 6. Configuration of the robust control strategy.

In the H_2 channel, $W_1(s)$ is a low-pass filter used to reject output disturbances while $W_2(s)$ is a high-pass filter or simply a small constant to prohibit excessive control efforts of controllers. $W_3(s)$ in the H_∞ channel is also a high-pass filter to guarantee robustness against system uncertainties. These filters are responsible for picking out the system dynamics within frequency range of interest. Moreover, the sensitivity transfer function between the disturbance input w and the measured output y can be formulated to measure the impact of a disturbance, as follows:

$$S(s) = \left(I - G(s)D(s)K(s)\right)^{-1} \tag{9}$$

Therefore, in the H_2 channel, the transfer matrix between w and z_2 is given by

$$T_{wz_2}(s) = \begin{bmatrix} W_1(s)S(s) \\ W_2(s)K(s)S(s) \end{bmatrix} \tag{10}$$

By minimizing the H_2 norm $\|T_{wz_2}(s)\|_2$, the resultant LDCs will optimize the control effort as well as achieve output disturbance rejection. Accordingly, as for the H_∞ channel, the transfer function between w and z_∞ is given by

$$T_{wz_\infty}(s) = W_3(s)K(s)S(s) \tag{11}$$

Similarly, the closed-loop system can enhance the immunity of its stability by reducing the H_∞ norm $\|T_{wz_\infty}(s)\|_\infty$ in the presence of system uncertainties.

Considering the wide distribution of the AELs and the implementation reliability of the designed controllers [27], a multi-stage mixed H_2/H_∞ robust control strategy is proposed in this paper to design the decentralized LDCs in a sequential manner. Meanwhile, to effectively suppress the inter-area oscillations, the relevant inter-area modes should be located in the proper region of the complex plane, such as the D-contour shown in Fig. 7. Therefore, a multi-stage region pole placement (RPP) is proposed to step-by-step shift inter-area modes into the final desirable region. Specifically, each stage of the optimization updates the desirable region by gradually narrowing it, as illustrated in Fig. 7, so that the damping burden can be allocated for different LDCs. The shadow region confined by the D-contour in Fig. 7 can be described as an LMI and expressed as follows:

$$\begin{gathered} D = \left\{ z \in C : f_D(z) = L + zM + \bar{z}\bar{M} < 0 \right\} \\ L = \begin{bmatrix} -2\alpha & 0 & 0 \\ 0 & 0 & 0 \\ 0 & 0 & 0 \end{bmatrix} \; M = \begin{bmatrix} -2\alpha & 0 & 0 \\ 0 & \sin\theta & -\cos\theta \\ 0 & \cos\theta & \sin\theta \end{bmatrix} \end{gathered} \tag{12}$$

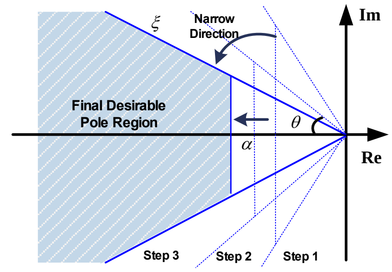

Fig. 7. Illustration of the multi-stage D-contour.

At each stage of the design, one LDC is derived by the proposed mixed H_2/H_∞ robust control strategy, which can be formulated as follows:

$$\begin{aligned} \min_{K(s)} \quad & \omega_\infty \left\|T_{wz_\infty}(s)\right\|_\infty^2 + \omega_2 \left\|T_{wz_2}(s)\right\|_2^2 \\ s.t. \quad & \boldsymbol{\lambda} \in D \end{aligned} \tag{13}$$

where ω_∞ and ω_2 are the weights for the H_∞ and H_2 performance, respectively. Here, these two weights make clear senses to impact final control results. For example, large ω_∞ will tend to enhance the robustness of the resultant LDCs against uncertainties but it possibly leads to relatively poor transient responses of the system and also excessive damping efforts from the controlled AELs; ω_2 however plays just opposite role in affecting the control results. Therefore, by using these general properties as the guideline, the trial and error method can also efficiently adjust ω_∞ and ω_2 to fulfill the desired control objectives [26]. $\boldsymbol{\lambda}$ is the set consisting of the closed-loop system's poles of concern.

B. Design Procedure of the Decentralized LDCs

1) *Small signal analysis of the open-loop power system*: Linearize the open-loop power system model at the nominal operating point, identify the critical inter-area modes, and select the most effective wide-area feedback signals for damping control;
2) *Shaping of the closed-loop system*: A reduced-order model $G(s)$ of the open-loop power system is obtained by the Schur method [28] to synthesize the low-order LDC. Three weighted filters in Fig. 6 are also chosen and the closed-loops are shaped;
3) *Solving the optimization model*: By adjusting the weights of ω_∞ and ω_2 in (13), robustness and control efforts of the closed-loop system can be flexibly and feasibly assigned. Then, via the *robust control toolbox* of MATLAB®, this optimization model (13) can be solved and the resultant robust LDC obtained.
4) *Iterative progress through nonlinear time domain simulations*: The control efforts of the resultant LDCs should be checked to see whether the controlled VDLs are excessively exerted. If so, the weights ω_∞ and ω_2 should be properly adjusted and Step 4 repeated until this issue is resolved. Similarly, the required damping effects and robustness can be obtained through the time domain simulations and iterative tuning of the weights.

Due to the sequential design, once a robust LDC is derived via Steps 1-4, the open-loop system model is updated and the RPP is also narrowed (Fig. 7). Those preparations precede the design of the next LDC, which follows the same steps.

V. Simulation Results and Analysis

The classic 5-area 16-machine test system (known as the New England and New York interconnected system [29]), as shown in Fig. 8, is used to exhibit the load damping effects presented in Section II and validate the proposed robust load damping control design. Three DFIG-based wind farms W1, W2, and W3 with capacities of 800, 800, and 1200 MW, respectively, are additionally connected at Bus-68, -39, and -18 in this benchmark system. All these wind farms are comprised of a same type of wind turbines with the active power capacity of 2 MW (the parameters of the wind turbine are shown in Appendix B). In particular, each wind farm is aggregately represented by a single wind turbine during the simulation, according to the aggregation method introduced in [30]. Moreover, the active power loads of Bus-68, -39, and -18 are increased by 800, 800, and 1200 MW, respectively [31]. Computing the eigenvalues of this modified system shows four poorly damped inter-area modes of oscillations (identified by M1, M2, M3, and M4).

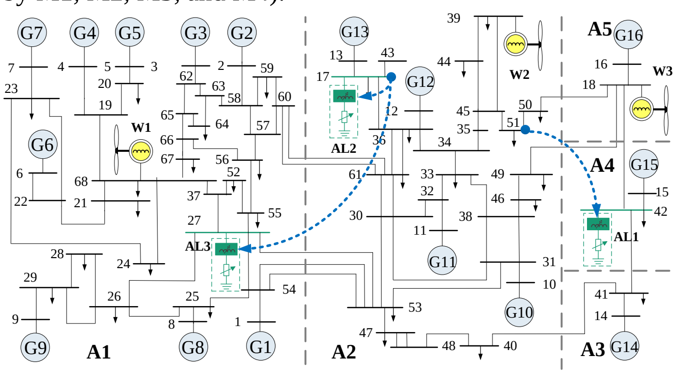

Fig. 8. Modified New England and New York interconnected system.

A. Investigation of Damping Effects from VDLs

Two operating conditions of the multi-machine system are employed in this investigation:

Case 1 – Stressed Condition: High gain (K_A=200) and insensitive excitation systems (T_e=0.36 s) [18] are used for all of the generators; one tie-line between Bus-53 and -54 and one tie-line between Bus-60 and -61 are switched off.

Case 2 – Normal Condition: All of the generators are equipped with excitation systems of the IEEE-DC1A type (K_A=20 and T_e=0.05 s) [18] and all of the loads are decreased by 10%.

Compared to CP loads, which consume constant power irrespective of terminal voltage deviations, CI loads are sensitive to terminal voltage. Therefore, it is assumed that all loads in the test system are composed of CI and CP loads with proportions β and (1-β), respectively. As β increases from 0 to 100%, the root loci of the four inter-area modes (eigenvalues) in the two cases move as depicted in Fig. 9, where arrows show the directions of the modes. The four inter-area modes in *Case 1* move to the right as β increases. Specifically, M1 and M2 even move to the unstable region. Such results demonstrate that, under stressed conditions, VDLs impair the damping of inter-area oscillations in power systems. In contrast, the leftward movements of the inter-area modes in *Case 2* indicate that VDLs in normal operating conditions have positive impacts on the inter-area modes.

Nonlinear time domain simulations are conducted to confirm the above modal analysis. After a small disturbance, Fig. 10 illustrates the oscillation curves for the angular speed (ω_{13}) of G13, voltage amplitude (V_{17}) of Bus-17, and active power consumption (P_{17}) of the CI loads at Bus-17. Clearly, ω_{13} and P_{17} are almost anti-phase when 100% CI loads are used in *Case 1*. According to Section II and Fig. 2, this indicates that the CI load at Bus-17 induces a negative damping torque on the shaft of G13 and thus weakens the damping of inter-area modes. However, Fig. 10 shows the phase difference between ω_{13} and P_{17} is less than 90° when 100% CI loads are also employed in *Case 2*. Therefore, the damping torque of G13 is additionally reinforced by the loads.

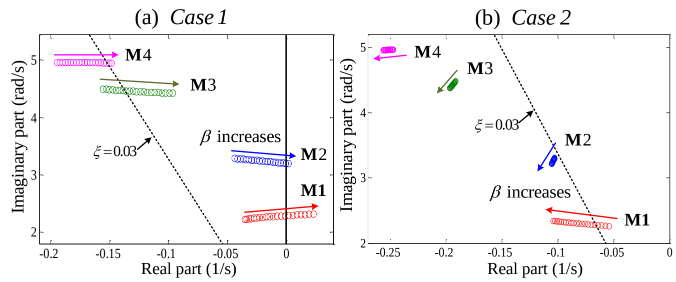

Fig. 9. Root loci of four inter-area modes in two cases.

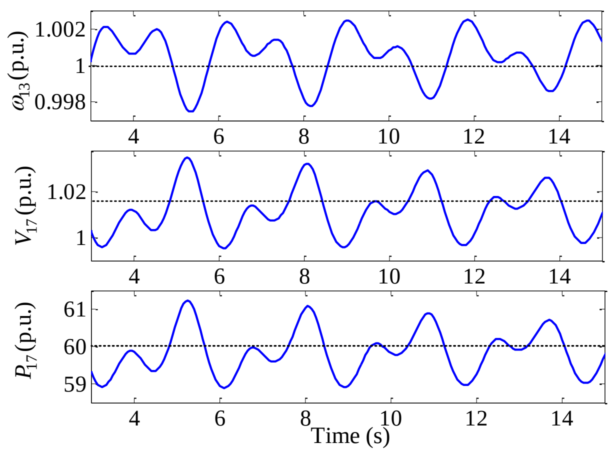

Fig. 10. Oscillation curves for *Case 1*.

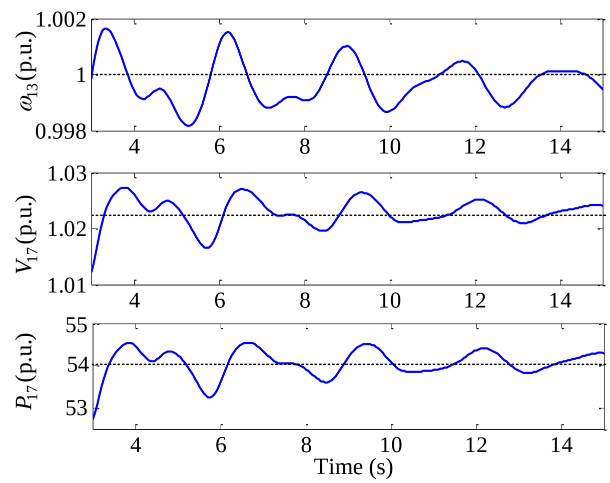

Fig. 11. Oscillation curves for *Case 2*.

B. *Application of Robust Decentralized LDCs*

Reference [29] specifically addresses the infeasibility of installing PSSs in the four largest machines (G13-G16) to damp the inter-area oscillations because these machines are actually aggregated models. Thus, the alternative solution proposed in this paper to modulate large-capacity VDLs (as an replacement of PSSs installed in G13-G16) for damping control is an exact fit for this test system.

It is supposed that three AELs (AL1, AL2, and AL3), selected as typical controllable VDLs, are integrated into the test system (Fig. 8). Specifically, three AELs hypothetically placing at Bus-17, -27 and -42, respectively, are just for validating the effectiveness of the proposed control design. In Area 4, the load replaced at Bus-42 by AL1 is 970 MW (out of the original 1850 MW); in Area 2, a portion (730 MW) of the original load (6000 MW) at Bus-17 is replaced by AL2; and, in Area 1, the original load connected at Bus-27 is replaced by AL3 with the same capacity of 640 MW. The models and parameters of the AELs are based on studies of an isolated power system in Inner Mongolia, China [11]. Moreover, each AEL is assumed to be accompanied by an MCR so that its terminal voltage can be rapidly and smoothly regulated. At the nominal operating point, power outputs of three wind turbines are supposed to be their expected values (EVs): 400, 400, and 600 MW, respectively.

Three damping controllers LDC1, LDC2, and LDC3, designed by the proposed strategy in Section IV, are locally installed with AL1-AL3, respectively. The voltage-phase angle δ_{51} of Bus-51 is selected as the feedback signal to LDC1 while the voltage-phase angle δ_{17} of Bus-17 is the effective feedback signal for LDC2 and LDC3, based on the residue analysis at the nominal operating point [28]. Thus, it is noted that the implemented damping control has employed a typical quasi-decentralized control architecture which is characterized by utilizing remote signals to enhance the effectiveness of controllers installed locally with controlled devices, such as VDLs [32]. The time delays of the feedback loops are commonly assumed to be 150 ms [33]. Additionally, the three weighted filters in Fig. 6 are given by

$$W_1(s)=\frac{30}{s+30} \qquad W_2(s)=0.5 \qquad W_3(s)=\frac{10s}{s+90} \tag{14}$$

The parameters (i.e. time constants) of these filters are selected according to their cut-off frequencies which should be decided by considering the frequencies of critical modes of interest [28]. For example, frequencies of inter-area power oscillations are generally (not strictly) lower than 1.5 Hz (e.g. the four concerned inter-area modes in the test system). According to the loop shape (Fig. 6), the cut-off frequencies of the low-pass and high-pass filters ($W_1(s)$ and $W_3(s)$) should be larger than 1.5 Hz. Therefore, as these filters are already selected to be first-order filters in order to reduce the computational complexity, their parameters are then readily calculated according to the cut-off frequencies. Moreover, the weights ω_∞ and ω_2 in the optimization model (13) are set to 0.55 and 0.45**,** respectively, to simultaneously account for the robustness and required damping performance. The three LDCs are sequentially synthesized by three stages, and the damping ratio used for constructing the gradually compressed LMI region (Fig. 7) is 0.1, 0.125, and 0.15, respectively, for these stages. By solving the optimization model (13), the transfer functions of three LDCs are obtained, as follows:

$$H_{\mathrm{LDC1}}(s)=0.76\frac{0.095s^4+10.12s^3-69.68s^2+25.87s+0.004}{s^4+1.701s^3+22.79s^2+20.82s+0.0005} \tag{15}$$

$$H_{\mathrm{LDC2}}(s)=0.56\frac{0.039s^4+5.659s^3+64.82s^2+14.57s+0.005}{s^4+3.084s^3+6.574s^2+0.032s} \tag{16}$$

$$H_{\mathrm{LDC3}}(s)=0.52\frac{3.726s^4+354.5s^3-1826s^2+4189s-795.8}{s^4+3.294s^3+75.81s^2+5.981s+2.402} \tag{17}$$

As a comparison to the proposed design, the case where the generators G1-G12 are equipped with local PSSs [29] for the damping control is simulated. Moreover, the local PSSs which use the generators' rotor speeds as the feedbacks signals are also optimized based on a modal decomposition method proposed in [34] where detailed information about this designed method can be found. At the nominal operating point, eigenvalues of the closed-loop power system are computed and shown in Table II (*operating point 1*). With the installation of the local PSSs, M1 and M3 are slightly shifted left and still poorly damped while the damping ratio of M4 is only 0.077 (less than the required value 0.15). However, the robust LDCs can make the damping ratios of all four inter-area modes sufficient (more than 0.15), which indicates the proposed design for VDLs is highly effective at enhancing damping ratios of inter-area modes.

Time domain simulations are conducted to further demonstrate the effectiveness of the proposed control strategy. An instantaneous three-phase short-circuit fault occurs at Bus 60 at 1.0 s that self-clears 100 ms later. In particular, the main purposed of using this fault is to drive the system states deviating from the equilibrium point so that the post-fault system dynamics can be utilized for the verification of control effects [29].The relative power angles of different generators can be used to clearly observe the dynamics of the four inter-area modes, as shown in Fig. 12. In the case with the local PSSs, the oscillations of M1 and M2 barely subside and the oscillations of M3 and M4 are slightly suppressed but do not disappear within 10 s. In the case with the proposed LDCs, however, the oscillations of four inter-area modes, especially M1 and M2, are all satisfactorily damped within 10 s.

Moreover, as mentioned in Section III-B, the control efforts of the robust LDCs should be evaluated to prevent excessive damping modulation and maintain safe operation of the controlled AELs. The dynamics of the active power consumed by AL1 to AL3 are plotted in Fig. 13, where the dashed horizontal lines denote their upper and lower boundaries specified for the power modulation. At the nominal operating point, the active power curves of AL1 to AL3 almost consistently stay within the boundaries, with the exception of the short fault period (100 ms). Compared to the case without any damping controller, the active power of AL1 to AL3 becomes more fluctuant due to the LDCs. Therefore, the controlled AELs must sacrifice their transient dynamic performance to meet the demands of the damping efforts. However, from a long-term viewpoint, quickly damped oscillations and stable operation of the system are the tradeoff for such sacrifices because the local PSS-controlled system (or the open-loop system) has unacceptable (even unstable) dynamics.

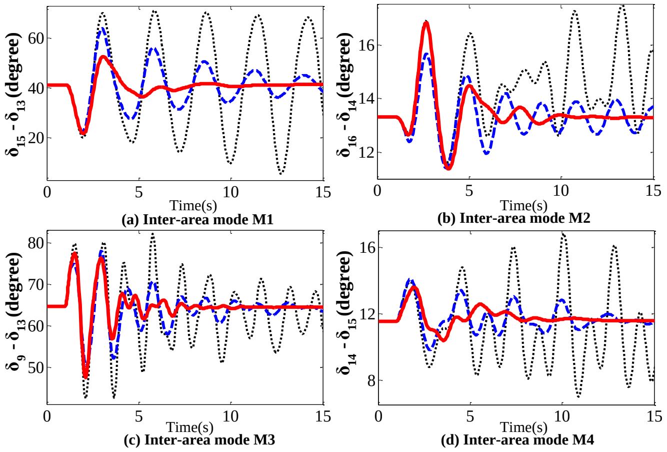

Fig. 12. Power angle oscillations (solid line: proposed robust LDCs; dotted line: local PSSs; dashed line: no controller).

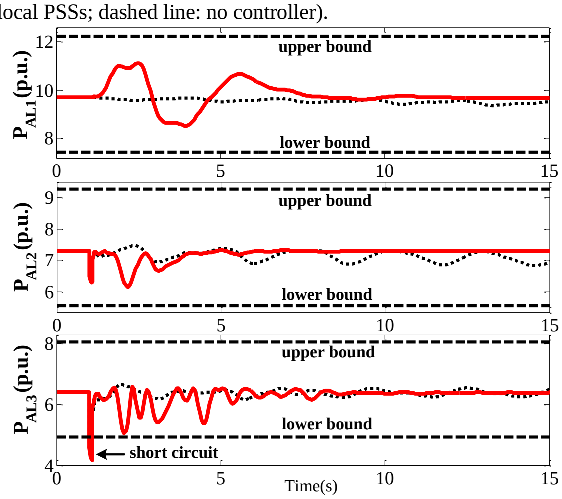

Fig. 13. Dynamics of active power consumed by AL1 to AL3 (solid line: proposed robust LDCs; dotted line: no controller).

C. Verification of Robustness

To verify the robustness of the LDCs, five representative operating points in terms of different wind generations and tie-line outages are simulated in this paper, as shown in Table I.

TABLE I
REPRESENTATIVE OPERATING POINTS

Operating point 1	Nominal operating point.
Operating point 2	Tie-line outage between buses 53-54; Total loads in Area 1 are increased by 5%; Power output of W1 is 800 MW and power outputs of W2 and W3 are the EVs.
Operating point 3	Tie-line outage between buses 18-49; Power outputs of W1 and W2 are the EVs and the power output of W3 is 1200 MW; The power of tie-line 18-50 increases from 1200 to 1800 MW.
Operating point 4	Power outputs of W1, W2, and W3 are 800, 800, and 100 MW, respectively.
Operating point 5	Tie-line outage between buses 60-61; Power outputs of the three WGs are all 100 MW; An instantaneous three-phase short-circuit fault happens in tie-line 40-41 at 1.0 s and is cleared 100 ms later by tripping this line without reclosing.

Eigenvalue analysis of the closed-loop power system under the five operating points is conducted, with the damping ratios of the inter-area modes shown in Table II. At all of the operating points, the damping performance of the robust LDCs is better than that of the local PSSs. Although damping ratios of some inter-area modes slightly decrease as the operating point deviates from the nominal one, they are still greater than 0.1 when the LDCs are installed. Nonlinear time domain simulations are also conducted, with the most inferior power angle dynamics of the inter-area modes at each operating point indicated in Fig. 14. Obviously, even under the emergent operating conditions (i.e., *operating points 2-5*), the LDCs outperform the local PSSs to provide quite satisfactory damping effects on the inter-area oscillations. In particular, due to the large energy of the disturbance (without reclosing fault tie-line 40-41) at *operating point 5*, the output of LDC1 is saturated and the active power of AL1 simultaneously reaches its floor (lower boundary), as shown in Fig. 15. Therefore, the above linear (eigenvalue) analysis and nonlinear simulation results are solid evidence of the excellent robustness of the proposed LDCs.

TABLE II
RESULTS OF EIGENVALUE ANALYSIS OVER MULTIPLE OPERATING POINTS

Operating Points		**Damping Ratios**			
		M1	**M2**	**M3**	**M4**
1	LDC	0.205	0.153	0.156	0.208
	PSS	0.064	0.034	0.060	0.077
2	LDC	0.209	0.154	**0.108**	0.199
	PSS	0.073	0.034	0.032	0.072
3	LDC	**0.147**	0.150	0.161	**0.168**
	PSS	0.012	0.132	0.116	0.148
4	LDC	0.178	**0.129**	0.186	0.205
	PSS	0.052	0.005	0.052	0.076
5	LDC	**0.100**	0.143	**0.122**	0.198
	PSS	0.013	0.044	0.034	0.114

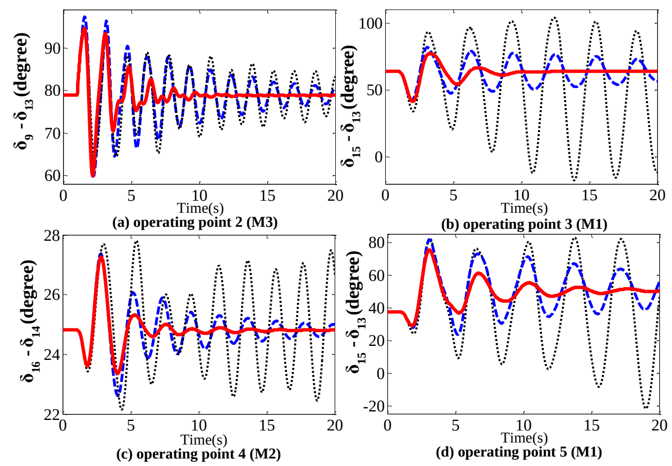

Fig. 14. Power angle oscillations at different operating points (solid line: proposed robust LDCs; dotted line: local PSSs; dashed line: no controller).

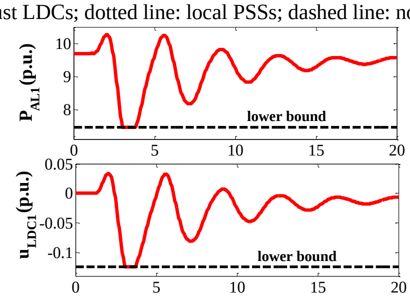

Fig. 15. Power output of AL1 and output of LDC1 at operating point 5.

D. Effects of Time Delays

To investigate the impacts of time delays on control effects of inter-area oscillation modes in power systems, simulations with different time delays are performed. As pointed out by [35] and [36], the communicating time delay is generally less than 300 ms for the wide-area control in practical power systems (e.g. China Southern Power Grid). Accordingly, five time delays are selected when the test system is at the nominal operating point, as shown in Table III. It can be found that the proposed LDCs show favorable robustness and have sufficient damping control performance subjected to different time delays. Meanwhile, because the time delay of 150 ms is considered during the design of LDCs (Subsection V-B), the damping ratios of the four inter-area modes are overall better than those in the other cases of time delays. Besides, the impacts of time delay on these modes are also dependent on their frequencies. As for M1, due to its lower frequency, the time delay can result in less phase lag of the wide-area feedback signal and consequently less adverse impacts. In contrast, the frequency of M3 is higher so that the time delay can cause more phase lag which obviously brings more impacts on the control results of this mode. Furthermore, the nonlinear time domain simulations also verify the above analysis, as shown in Fig. 16. Compared to the small distinctions among dynamic curves of δ_{15}-δ_{13} which are dominated by M1, the larger time delay induces more apparent fluctuant dynamics of δ_9-δ_{13} because the damping ratio of M3 is more obviously deteriorated.

TABLE III
EFFECTS OF DIFFERENT TIME DELAYS ON THE FOUR INTER-AREA MODES

Time Delays (ms)	Damping Ratios			
	M1	M2	M3	M4
0	0.203	0.154	0.141	0.182
75	0.208	0.155	0.150	0.193
150	0.205	0.153	0.156	0.208
225	0.197	0.150	0.127	0.187
300	0.186	0.145	0.098	0.158

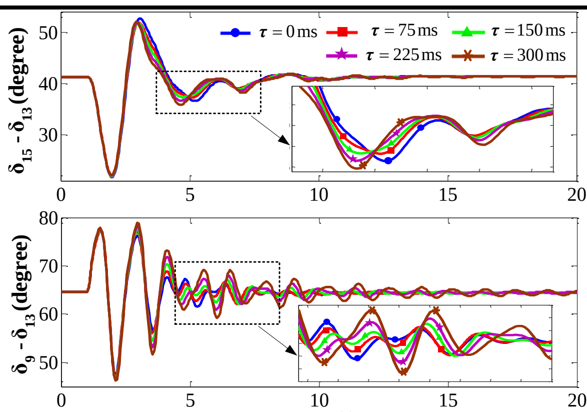

Fig. 16. Power angle oscillations dominated by M1/M3 under different time delays.

The robustness of proposed LDCs against time-varying delays is also simulated. The dynamic of active power carried by the key tie-line 53-54 is typically selected and illustrated in Fig. 17. It is seen that when the time delay is changed from 225 ms to 300 ms the power oscillation will quiet down with relatively slow speed. However, as the time delay decreases to 150 ms, the power oscillation can be quickly damped. Particularly, missing communication data is also a common yet inevitable issue which may obviously deteriorate the control effects. Thus design of damping controllers which are robust against the feedback data missing is an important direction to improve the studies of this paper in the future.

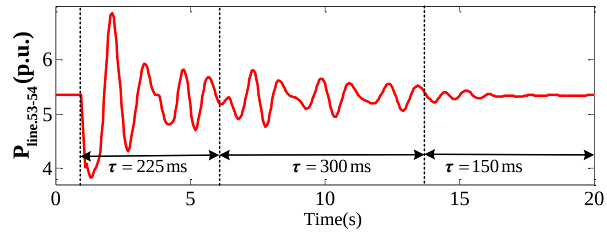

Fig. 17. The oscillation of active power in the key tie-line 53-54 with time-varying delays.

VI. Conclusion

This paper mathematically investigates the mechanism of the influence of VDLs on inter-area oscillations in power systems by complex torque analysis. It concludes that, under stressed system operating conditions, the VDL is more likely to deteriorate inter-area modes. To address this issue, a novel damping control architecture based on typical large-scale VDLs, i.e., AELs, is proposed to improve the damping of inter-area oscillations. Specifically, such architecture uses the decentralized wide-area LDCs to supplementarily control the AELs. Moreover, a multi-stage robust design method is applied to synthesize the LDCs. Simulation results conducted on the modified New England and New York interconnected system validate the correctness of the torque analysis and verify the effectiveness and robustness of the proposed load damping control strategy. Hence, the proposed damping control for large-scale VDLs can be regarded as a potential solution to the challenging issue of poorly-damped inter-area oscillations in modern power systems.

Appendix

A. Definitions of K_1-K_6 Coefficients

According to the linearization process shown in [18]-[20], the SMIB model in Fig. 1 can be linearized based on following coefficients:

$$
\begin{aligned}
K_1 &= \frac{X_q - X_d'}{X_d' + X_t} i_{q0} V \sin\delta_0 + \frac{V\cos\delta_0}{X_q + X_t} E_{q0} \\
K_2 &= \frac{X_q + X_t}{X_d' + X_t} i_{q0} \qquad K_3 = \frac{X_d' + X_t}{X_d + X_t} \\
K_4 &= \frac{X_d - X_d'}{X_d' + X_t} V \sin\delta_0 \\
K_5 &= \frac{V}{V_{t0}} \left(\frac{X_q}{X_q + X_t} V_{td0} \cos\delta_0 - \frac{X_d'}{X_d' + X_t} V_{tq0} \sin\delta_0 \right) \\
K_6 &= \frac{V_{tq0}}{V_{t0}} \frac{X_t}{X_d' + X_t}
\end{aligned} \tag{18}
$$

where X_d and X_q are the d-axis and q-axis synchronizing reactances, respectively, of the generator and X_d' is the transient reactance; X_t is the external reactance; δ is the rotor angle of the generator; i_q is the q-axis component of stator current; V_{td}

and V_{tq} are the d-axis and q-axis components, respectively, of the terminal voltage V_t. The subscript '0' means that the associated variables are calculated as the system is at the steady state. It can be found that the coefficient K_5 can be either positive or negative, which is related to the operating condition of the system. For instance, when the system load is heavy, the rotor angle δ will be large and consequently lead to negative K_5.

B. Parameters of the Wind Turbine Generator

This paper employs the DFIG-based wind turbine with the structure given in [37] and the parameters on base of machine ratings 2.24 MVA and 690 V as follows: cut-in wind speed ω_{c-in} = 4 m/s; rated wind speed ω_{rate} = 13 m/s; cut-out wind speed ω_{c-out} = 25 m/s; wind turbine radius R = 46.7 m; stator winding resistance R_s = 0.0116 p.u.; stator inductance L_s = 0.0229 p.u.; inertia time constant of wind turbine H_t = 3.9 s; damping coefficient D_{tw} = 0.02 p.u..

REFERENCES

[1] M. Klein, G. J. Rogers, and P. Kundur, "A fundamental study of inter-area oscillations in power systems," *IEEE Trans. Power Syst.*, vol. 6, no. 3, pp. 914-921, Aug. 1991.

[2] J. V. Milanovic, I. A. Hiskens, "Oscillatory interaction between synchronous generator and local voltage-dependent load," *IEE Proc.-Gener. Transm. Distrib*, vol. 142, no. 5, pp. 473-480, Sep. 1995.

[3] Z. Akhtar, B. Chaudhuri, and S. Y. R. Hui, "Primary frequency control contribution from smart loads using reactive compensation," *IEEE Trans. Smart Grid*, vol. 6, no. 5, pp. 2356-2365, Sep. 2015.

[4] T. Cui, W. Lin, Y. Sun, *et al.*, "Excitation voltage control for emergency frequency regulation of island power systems with voltage-dependent loads," *IEEE Trans. Power Syst.*, vol. 31, no. 2, pp. 1204-1217, Mar. 2016.

[5] H. Jiang, J. Lin, Y. H. Song, *et al.*, "Demand side frequency controls scheme in an isolated wind power system for industrial aluminum smelting production," *IEEE Trans. Power Syst.*, vol. 29, no. 2, pp. 844-853, Mar. 2014.

[6] J. Liu, W. Zhang, and Y. Liu, "Primary frequency response from the control of LED lighting loads in commercial buildings," *IEEE Trans. Smart Grid*, vol. 8, no. 6, pp. 2880-2889, Nov. 2017.

[7] O. Samuelsson and B. Eliasson, "Damping of electro-mechanical oscillations in multimachine system by direct load control," *IEEE Trans. Power Syst.*, vol. 12, no. 4, pp. 1604-1609, Nov. 1997.

[8] I. Kamwa, R. Grondin, D. Asber, *et al.*, "Active-power stabilizers for multimachine power systems challenges and prospects," *IEEE Trans. Power Syst.*, vol. 13, no. 4, pp. 1352-1358, Nov. 1998.

[9] I. Kamwa, R. Grondin, D. Asber, *et al.*, "Large-scale active-load modulation for angle stability improvement," *IEEE Trans. Power Syst.*, vol. 14, no. 2, pp. 582-590, May. 1992.

[10] B. Ramanathan and V. Vittal, "Small-disturbance angle stability enhancement through direct load control part I—framework development," *IEEE Trans. Power Syst.*, vol. 21, no. 2, pp. 773-781, May. 2006.

[11] J. Xu, S. Liao, Y. Sun, *et al.*, "An isolated industrial power system driven by wind-coal power for aluminum productions: a case study of frequency control," *IEEE Trans. Power Syst.*, vol. 30, no. 1, pp. 471-483, Jan. 2015.

[12] M. Beiraghi, A. M. Ranjbar, "Additive model decision tree-based adaptive wide-area damping controller design," *IEEE System Journal*, to be published.

[13] T. Wang, Z. Wang, J. Liu, J. S. Thorp, and Y. Yang, "Classification and regression tree-based adaptive damping control of inter-area oscillations using wide-area signals," *IET Gener. Transm. Distrib.*, vol. 8, no. 9, pp. 4297–4309, Nov. 2016.

[14] D. Ke and C. Y. Chung, "Design of probabilistically-robust wide-area power system stabilizers to suppress inter-area oscillations of wind integrated power systems," *IEEE Trans. Power Syst.*, vol. 31, no. 6, pp. 471-483, Jan. 2015.

[15] X. M. Mao, Y. Zhang, and X. C. Wu, "Coordinated control of interarea oscillation in the China Southern Power Grid," *IEEE Trans. Power Syst.*, vol. 21, no. 2, pp. 845-852, May. 2006.

[16] S. Elenius, K. Uhlen, and E. Lakervi, "Effects of controlled shunt and series compensation on damping in the Nordel System," *IEEE Trans. Power Syst.*, vol. 20, no. 4, pp. 1946-1957, Nov. 2005.

[17] J. Fang, W. Yao, Z. Chen, *et al.*, "Design of anti-windup compensator for energy storage-based damping controller to enhance power system stability," *IEEE Trans. Power Syst.*, vol. 29, no. 3, pp. 1175-1185, May. 2014.

[18] P. Kundur, *Power System Stability and Control*. New York: McGraw-Hill, 1994.

[19] A. Kumar, "Power system stabilizers design for multimachine power systems using local measurements," *IEEE Trans. Power Syst.*, vol. 31, no. 3, pp. 2163-2171, May. 2016.

[20] F. P. deMello and C. Concordia, "Concepts of synchronous machine stability as affected by excitation control," *IEEE Trans. Power Apparatus and Systems*, vol. PAS-88, no. 4, pp. 316-329, Apr. 1969.

[21] P. Pourbeik and M. J. Gibbard, "Damping and synchronizing torques induced on generators by FACTS stabilizers in multimachine power systems," *IEEE Trans. Power Syst.*, vol. 11, no. 4, pp. 1920-1925, Nov. 1996.

[22] M. Tian, "Design and simulation of a voltage-control system with a controllable reactor of transformer type," in *Proc. IEEE Conf. Ind. Technol., ICIT*, Hong Kong, 2005, pp. 419-423.

[23] J. Yuan, J. Zhou, B. Chao, *et al.*, "A novel compact high-voltage test system based on a magnetically controlled resonant transformer," *IEEE Trans. Magn.*, vol.51, no.11, Nov. 2015, Art. ID 1700204.

[24] L. Liang, Y. Hou, and D. J. Hill, "Enhancing Flexibility of An Islanded Microgrid with Electric Springs," *IEEE Trans. Smart Grid*, to be published.

[25] C. Scherer, P. Gained, and M. Chilali, "Multiobjective output-feedback control via LMI optimization," *IEEE Trans. Autom. Control*, vol. 42, no. 7, pp. 896-911, Jul. 1997.

[26] Y. Zhang and Anjan Bose, "Design of wide-Area damping controllers for interarea oscillations," *IEEE Trans. Power Syst.*, vol. 23, no. 3, pp. 1136-1143, Jul. 2008.

[27] B. Chaudhuri, B. C. Pal, A. C. Zolotas, *et al.*, "Mixed-sensitivity approach to H_∞ control of power system oscillations employing multiple FACTS devices," *IEEE Trans. Power Syst.*, vol. 18, no. 3, pp. 1149-1156, Aug. 2003.

[28] B. Pal and B. Chaudhuri, *Robust Control in Power Systems*, New York: Springer, 2005.

[29] C. Canizares, T. Fernandes, E. Geraldi, *et al.*, "Benchmark models for the analysis and control of small-signal oscillatory dynamics in power systems," *IEEE Trans. Power Syst.*, vol. 32, no. 1, pp. 715-722, Jan. 2017.

[30] E. Muljadi, C. P. Butterfield, A. Ellis, *et al*., "Equivalencing the collector system of a large wind power plant," in *Proc. IEEE Power Eng. Soc. Gen. Meeting*, Montreal, Canada, 2006, pp. 1-8.

[31] W. Du, J. Bi, J. Cao and H. F. Wang, "A method to examine the impact of grid connection of the DFIGs on power system electromechanical oscillation modes," *IEEE Trans. Power Syst.*, vol. 31, no. 5, pp. 3775-3784, Sep. 2016.

[32] D. Dotta, A. S. Silva, and I. C. Decker, "Wide-area measurements-based two-level control design considering signal transmission delay," *IEEE Trans. Power Syst.*, vol. 24, no. 1, pp. 208-216, Feb. 2009.

[33] M. Beiraghi and A. M. Ranjbar, "Adaptive delay compensator for the robust wide-area damping controller design," *IEEE Trans. Power Syst.*, vol. 31, no. 6, pp. 4966-4976, Nov. 2016.

[34] J. Zhang, C. Y. Chung, and Y. Han, "A novel modal decomposition control and its application to PSS design for damping interarea oscillations in power systems," *IEEE Trans. Power Syst.*, vol. 27, no. 4, pp. 2015-2025, Nov. 2012.

[35] C. Lu, X. Zhang, X. Wang, and Y. Han, "Mathematical expectation modeling of wide-area controlled power systems with stochastic time delay," *IEEE Trans. Smart Grid*, vol. 6, no. 3, pp. 1511-1519, May. 2015.

[36] K. Zhu, M. Chemome, L. Nordstrom, S. Holmstrom, and G. Ericsson, "Design requirements of wide-area damping systems—using empirical data from a utility IP network," *IEEE Trans. Smart Grid*, vol. 5, no. 2, pp. 829-838, May. 2014.

[37] C. Zhang, D. Ke, Y. Sun, C. Y. Chung, J. Xu, and F. Shen, "Coordinated supplementary damping control of DFIG and PSS to suppress inter-area

oscillations with optimally controlled plant dynamics," *IEEE Trans. Sustain. Energy*, vol. 9, no. 2, pp. 780-791, April. 2018.

Chen Zhang (S'16) received the B.S degree in Electrical Engineering in 2014 from Wuhan University, Wuhan, China. Currently, he is pursuing the Ph.D. degree in the School of Electrical Engineering, Wuhan University. At present, he is also funded by Chinese Scholarship Council (CSC) as a joint Ph.D. student in the Department of Electrical Engineering and Computer Science, Case Western Reserve University, Cleveland, Ohio, USA.

His research interests are in power system stability and control, wind power, and direct load control.

Deping Ke received the B.S degree in Electrical Engineering in 2005 from Huazhong University of Science and Technology, Wuhan, China, and the Ph.D. degree in Electrical Engineering from The Hong Kong Polytechnic University in 2012. Currently, he is an Associate Professor with the School of Electrical Engineering, Wuhan University, China.

His research interests are in power system dynamics and control, and economic operation of power systems.

Yuanzhang Sun (M'99-SM'01) received the B.S. degree from Wuhan University of Hydro and Electrical Engineering, Wuhan, China, in 1987, the M.S. degree from the Electric Power Research Institute(EPRI), Beijing, China, in 1982, and the Ph.D. degree in electrical engineering from Tsinghua University, Beijing, in 1988.

Currently, he is a Professor of the School of Electrical Engineering at Wuhan University, and a Chair Professor of the Department of Electrical Engineering and Vice Director of the State Key Lab of Power System Control and Simulation at Tsinghua University. His main research interests are in the areas of power system dynamics and control, wind power, voltage stability and control, and reliability.

C. Y. Chung (M'01–SM'07–F'16) received the Ph.D. degree in electrical engineering from The Hong Kong Polytechnic University in 1999. He is currently a Professor and the SaskPower Chair in Power Systems Engineering in the Department of Electrical and Computer Engineering at the University of Saskatchewan, Saskatoon, SK, Canada.

His research interests include power system stability/control, smart grid technologies, renewable energy, computational intelligence applications, power markets, and electric vehicle charging.

Dr. Chung is an Editor of the *IEEE Transactions on Power Systems* and *IEEE Transactions on Sustainable Energy*. He is also a Member-at-Large (Smart Grid) of IEEE PES Governing Board and the IEEE PES Region 10 North Chapter Representative.

Jian Xu (M'08) received the Ph.D. degree in electrical engineering from the Wuhan in 2007. He joined Wuhan University as a Lecturer in 2007. Since 2015, he has been a Professor of the School of Electrical Engineering at Wuhan University. During 2013–2014, he was a visiting scholar at the Energy Systems Innovation Center, Washington State University, Pullman, WA, USA.

His research interests include power system stability and control, wind power, and voltage stability.